Journal of Materials Chemistry C

ROYAL SOCIETY OF CHEMISTRY

PAPER

View Article Online
View Journal | View Issue

Cite this: J. Mater. Chem. C, 2024, 12, 1516

Sodalite-like carbon based superconductors with T_c about 77 K at ambient pressure†

Siyu Jin, ‡[a] Xiaoyu Kuang, ‡[a] Xilong Dou,[a] Andreas Hermann *[b] and Cheng Lu *[c]

Received 8th November 2023,
Accepted 17th December 2023

DOI: 10.1039/d3tc04096h

rsc.li/materials-c

The attainment of superconductivity at room temperature is a longstanding aspiration for both experimental and theoretical scientists. Materials exhibiting superconductivity under ambient conditions would have significant applications. Here, we report two metastable phases of sodalite-like carbon based superconductors, GaC_6 and GeC_6, at ambient pressure using the CALYPSO structural search method and first-principles calculations. Our calculations reveal that both GaC_6 and GeC_6 compounds have $Im\bar{3}m$ symmetry and are dynamically stable at ambient pressure with T_c values up to the boiling point of liquid nitrogen. The underlying mechanisms indicate that the guest Ga and Ge atoms play a dual role in enhancing the structural stability and concurrently acting as electron donors, thereby modulating the electronic properties of the C_{24} covalent frameworks, *i.e.* from insulating states to superconducting states. The present results offer insights into the exploration of novel high temperature superconductors under ambient conditions.

1 Introduction

Since Onnes firstly observed the superconductivity in solid mercury,[1] it has commanded sustained attention within the scientific community.[2–4] In the subsequent decades, superconductivity was observed in numerous other materials. In 1913, the superconducting state was identified in lead with a T_c of 7 K, while in 1941, niobium nitride was demonstrated to be a superconductor at 16 K. Great efforts have been dedicated to the pursuit of superconductivity at increasing temperatures, with the ultimate objective of achieving a room-temperature superconductor. An enormous step forward was the discovery of unconventional superconductivity in the cuprates, which allowed constructing devices cooled by liquid nitrogen.[5,6] Recently, conventional phonon-mediated superconductors have made tremendous progress.[7–25] As a light-element compound, sulfur hydride, namely H_3S, is confirmed to be a superconductor with an extremely high T_c value of 203 K at high pressures.[25] Subsequently, hydrogen-rich clathrates in rare earth hydrides were discovered to exhibit ultra-high T_c superconductivity due to the strong electron–phonon coupling (EPC), which is related to the motions of H atoms within the cages and the larger electron densities contributed by H atoms at the Fermi level.[26–28] However, the endeavors to synthesize these superhydrides are constrained by the current technological capabilities. Consequently, the strategies for procuring high T_c superconductors under moderate pressures have garnered widespread attention.[29]

The clathrate motif of atomic hydrogen is unlikely to persist at low or ambient pressure. Stronger bound clathrate cages offer more promising routes towards ambient pressure stability. In fact, some non-hydrogen clathrates connected by sp^3 hybridized C–C covalent bonds also exhibit superconductivity at moderate or even ambient pressure. Typically, fullerene (C_{60}) is considered to be a semiconductor under ambient conditions and the energy gap is approximately 1.6 eV to 1.7 eV.[30] However, when doped with appropriate atoms, such as alkali metals, fullerenes can become conductive or even exhibit superconductivity.[31–33] The corresponding T_c values increase with the cell volume of alkali metal doped fullerenes. Under ambient conditions, the T_c of $RbCs_2C_{60}$, characterized by a face-centered-cubic structure, is found to be 33 K,[31] which is the highest T_c value among those of the trivalent alkali metal doped fullerenes (A_3C_{60}).[31,32] In contrast, the doped fullerene of Cs_3C_{60}, notable for its non-cubic crystalline arrangement, does not exhibit superconductivity under ambient pressure. Interestingly, when Cs_3C_{60} transforms into a cubic structure at high pressure, its T_c reaches 40 K at 15

[a] Institute of Atomic and Molecular Physics, Sichuan University, Chengdu 610065, China
[b] Centre for Science at Extreme Conditions and SUPA, School of Physics and Astronomy, University of Edinburgh, Edinburgh EH9 3FD, UK. E-mail: a.hermann@ed.ac.uk
[c] School of Mathematics and Physics, China University of Geosciences (Wuhan), Wuhan 430074, China. E-mail: lucheng@calypso.cn

† Electronic supplementary information (ESI) available: Phonon dispersion curves, bond length, Bader charge, COHP calculations, electronic band structures and densities of states, and EPC calculations of XC_6 compounds. See DOI: https://doi.org/10.1039/d3tc04096h

‡ S.-Y. J. and X.-Y. K. contributed equally to this work.

kbar.[33] Similarly, the face-centered cubic (FCC) C_{34} clathrate transforms from an insulating state to a metallic state after the intercalations of fluorine atoms, which introduces hole carriers into the top valence bands of the host carbon frameworks. The fluorine-doped carbon clathrate (FC_{34}) is predicted to exhibit high temperature superconductivity with a T_c value of 77 K at ambient pressure.[34] Thus, the lattice arrangement with cubic or approximate cubic symmetry is determined as a pivotal determinant in the pursuit of relatively high T_c values, potentially providing novel avenues for the discovery of high temperature superconductors under ambient conditions.

Recent computational studies have explored the superconducting behaviors of mixed boron-carbon based clathrates at ambient pressure,[35] a class of materials that have been shown to be recoverable following high-pressure synthesis.[36] Interestingly, the T_c values of these binary-guest configurations are adjustable through the manipulations of the guest metal atoms, which are attributed to the rigid band behaviors of the sp^3 hybridized B–C covalent frameworks in boron-carbon clathrates. Pure carbon clathrates are arguably simpler materials, but have not been synthesized yet. However, they have been studied computationally, including doping with simple metal ions (akin to the fullerene superconductors).[37,38] Most importantly, the sodalite-like NaC_6 is predicted to be a superconductor with a high T_c value.[39] A systematic study of this family of materials is still missing. This inspired us to further explore the superconductivities and underlying mechanisms of sp^3-bonded C_6 clathrates with different guest atoms. In the present work, we carry out systematic high-throughput density functional theory (DFT) calculations to search for stable sp^3-bonded C_6 clathrates at ambient pressure and then determine their electronic and superconducting properties. Phonon calculations show that many XC_6 compounds (X = Ni, Cu, Zn, Ga, Ge, As, Se, Br, Ru, Rh, Pd, Ag, Cd and I) with $Im\bar{3}m$ symmetry are dynamically stable, including guest atoms ranging from transition metals *via* p-block elements to the halogens (see Fig. S1, ESI†). Among them, substantial charge transfers in GaC_6 and GeC_6 clathrates are observed due to the interactions between metal Ga/Ge atoms and C_{24} cages, the respective values of which are 0.12 *e* and 0.13 *e* per C atom. The electron phonon coupling (EPC) calculations reveal that GaC_6 exhibits a T_c value of 82 K, while GeC_6 demonstrates a T_c value of 76 K.

2 Computational details

High-throughput structural searches of carbon based clathrates at ambient pressure are conducted through the CALYPSO[40,41] method and density functional theory (DFT) calculations. The crystal structure searches for GaC_6 ranging from 1 to 4 f.u. per cell have been performed at ambient pressure. Over 5000 structures have been generated in total. The structural optimizations and the phonon dispersion curve are calculated using the Vienna *Ab initio* Simulation Package (VASP) package.[42–44] The cutoff energy is chosen as 600 eV and the smallest allowed spacing is chosen as 0.2 $Å^{-1}$ between *k* points. In addition, tighter setting parameters are used for the phonon mode simulations.[45] EPC calculations are performed using the QUANTUM ESPRESSO code[46] based on density functional perturbation theory (DFPT). Ultrasoft pseudopotentials of Perdew–Burke–Ernzerhof formula are adopted to calculate the EPC interactions. The cutoff energy and the charge density cutoff are chosen as 100 Ry and 1000 Ry after the convergence test, respectively. The EPC calculations employ a *q*-mesh of 6 × 6 × 6 in the first Brillouin zone. A *k*-mesh of 24 × 24 × 24 was used to ensure that the sampling of *k*-points achieved convergence. Taking into account the significant difference in atomic mass between carbon and metal atoms, Gor'kov and Kresin (G–K) divide the phonon spectrum into two regions: optical and acoustic phonons. We can introduce the coupling constants λ_{opt} and λ_{ac} to characterize the relative contribution of the acoustic and optical branches to the total electron–phonon coupling strength.[47,48] In common metals, the function $\alpha^2F(\omega)$ is characterized by a peak in the phonon density of states. Such fact permits the replacement of $\omega(q)$ in the phonon propagator by its average value $\tilde{\omega}^2 = \langle\omega^2\rangle^{1/2}$. At $T = T_c$, the order parameter can be written as:

$$\Delta(\omega_n)Z = \pi T\sum_m\left[\frac{{\tilde{\omega}_{opt}}^2}{(\omega_n-\omega_m)^2+{\tilde{\omega}_{opt}}^2}\times\left(\lambda_{opt}-\mu^*\right)+\frac{{\tilde{\omega}_{ac}}^2}{(\omega_n-\omega_m)^2+{\tilde{\omega}_{ac}}^2}\times\lambda_{ac}\right]\frac{\Delta\omega_m}{\omega_m} \quad (1)$$

the electron–phonon coupling λ is given by

$$\begin{aligned}\lambda &= \lambda_{opt}+\lambda_{ac}\\ &= 2\int_0^{\omega_{amax}}\frac{\alpha^2F(\omega)}{\omega}d\omega\\ &\quad+2\int_{\omega_{amax}}^{\omega_{omax}}\frac{\alpha^2F(\omega)}{\omega}d\omega\end{aligned} \quad (2)$$

In eqn (2), the ω_{amax} and ω_{omax} represent the maximum frequency of acoustic and optical models, respectively. Here, it is defined as follows:

$$\begin{aligned}\langle{\omega_{ac}}^2\rangle &= \frac{2}{\lambda_{ac}}\int_0^{\omega_{amax}}\omega^2\frac{\alpha^2F(\omega)}{\omega}d(\omega)\\ &= \frac{2}{\lambda_{ac}}\int_0^{\omega_{amax}}\omega\times\alpha^2F(\omega)d(\omega)\end{aligned} \quad (3)$$

$$\begin{aligned}\langle{\omega_{opt}}^2\rangle &= \frac{2}{\lambda_{opt}}\int_{\omega_{amax}}^{\omega_{omax}}\omega^2\frac{\alpha^2F(\omega)}{\omega}d(\omega)\\ &= \frac{2}{\lambda_{opt}}\int_{\omega_{amax}}^{\omega_{omax}}\omega\times\alpha^2F(\omega)d(\omega)\end{aligned} \quad (4)$$

In case $\lambda_{ac} \ll \lambda_{opt}$, and assuming that:

$$T_c = T_c^{opt} + \Delta T_c^{ac}, \text{ and } T_c^{opt} \gg \Delta T_c^{ac} \quad (5)$$

the T_c can be identified by using the following equation:

$$T_c = \left[1 + 2\frac{\lambda_{ac}}{\lambda_{opt} - \mu^*} \times \frac{1}{1 + \rho^{-2}}\right] T_c^0, \quad \rho = \frac{\tilde{\omega}_{ac}}{\pi T_c^0}, \quad T_c^0 \equiv T_c^{opt} \tag{6}$$

where T_c^0 is the transition temperature contributed by the coupling between the electrons and the optical models. For $\lambda_{opt} \leq 1.5$, it is defined as follows:

$$T_c^0 = \frac{\tilde{\omega}_{opt}}{1.2} \exp\left[-\frac{1.04(1 + \lambda_{opt})}{\lambda_{opt} - \mu^*(1 + 0.62\lambda_{opt})}\right] \tag{7}$$

For $\lambda_{opt} > 1.5$, it is given by:

$$T_c^0 = \frac{0.25\tilde{\omega}_{opt}}{\left[e^{\frac{2}{\lambda_{eff}}} - 1\right]^{1/2}} \tag{8}$$

where λ_{eff} is given by:

$$\lambda_{eff} = (\lambda_{opt} - \mu^*)\left[1 + 2\mu^* + \lambda_{opt}\mu^* t(\lambda_{opt})\right]^{-1}, \quad t(x) = 1.5\exp(-0.28)x \tag{9}$$

3 Results and discussion

Fig. 1(a) depicts the crystal structure of GaC_6 at ambient pressure. The host carbon clathrate displays a structural composition comprising six square C4 rings and six hexagonal C6 rings, resembling the structure of sodalite. The guest Ga atoms are located at the center of the cubic unit, forming a body-centered cubic structure with $Im\bar{3}m$ symmetry. Table S1 (ESI†) summarizes the C–C and Ga–C bond lengths of GaC_6. Specifically, the C–C bond lengths in GaC_6 are 1.640 Å, while the Ga–C bond lengths are 2.593 Å. The C–C bond length is significantly elongated compared to the pure C-sodalite (no guest), where it is 1.543 Å.

Fig. 1(b) illustrates the electron localization function (ELF)[49,50] of GaC_6. It can be seen that the valence electrons of the C atoms are primarily localized on the C–C bonds, forming strong covalent σ bonds. In contrast, the valence electrons of the guest Ga atoms are concentrated near the atoms. This phenomenon indicates that in GaC_6, each C atom is linked to other four carbon atoms through sp^3 hybridized covalent bonds, creating two types of bond angles: 90° and 120° (*e.g.*, ∠C2–C1–C3 and ∠C3–C1–C4). Meanwhile, the guest Ga atoms are encapsulated in the C cages with weak interactions between Ga atoms and C atoms. However, the guest atoms play a pivotal role in buttressing the structures and wield the capacity to regulate the electrons of C_{24} covalent frameworks.

The Bader charges[51] of the GaC_6 indicate a slight charge transfer between the guest Ga atoms and the C atoms. Each C atom accepts about 0.12 *e* from the guest atom, indicating that the C atoms act as the electron acceptors in GaC_6, since each C atom forms a strong covalent bond with four adjacent C atoms, and the four valence electrons of the C atom are firmly bound within the C_{24} cage.

The Crystal Orbital Hamilton Population (COHP) analysis[52,53] for GaC_6 is depicted in Fig. S2 and Table S1 (ESI†). The negative projected COHP (–pCOHP) and the negative integrated COHP (–ICOHP) of both Ga–C and covalent C–C pairs are presented. The –ICOHP values of C–C bonds are 7.44 eV per atom pair, an order of magnitude higher than those of Ga–C bonds (0.61 eV per atom pair), suggesting that the C–C bonds are considerably stronger than the Ga–C bonds, in agreement with the above ELF results. It can be seen from Fig. S2 (ESI†) that the Ga–C bonds in GaC_6 exhibit almost no anti-bonding states below the Fermi level, which is beneficial to the stability of the structure. In contrast, for example in the AgC_6 and NiC_6 compounds, the regions of the d orbitals of Ag and Ni atoms contributing to the density of states show visibly anti-bonding states, indicating that the aggregation of energy bands contributed by the d orbitals of transition metal atoms is detrimental to the stabilities of the compounds (see Fig. S3, ESI†).

To gain further insights into the electronic properties of GaC_6, we perform the electronic band structure, projected electronic density of states (PDOS), Fermi surfaces and EPC calculations. The results are shown in Fig. 2. The band structure visualizes the electron doping from Ga into the C-sublattice.

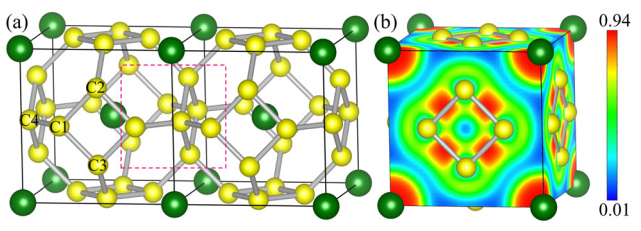

Fig. 1 (a) Crystal structure of GaC_6, the Ga and C atoms are represented by green and yellow balls, respectively. (b) The electron localization functions (ELF) for GaC_6.

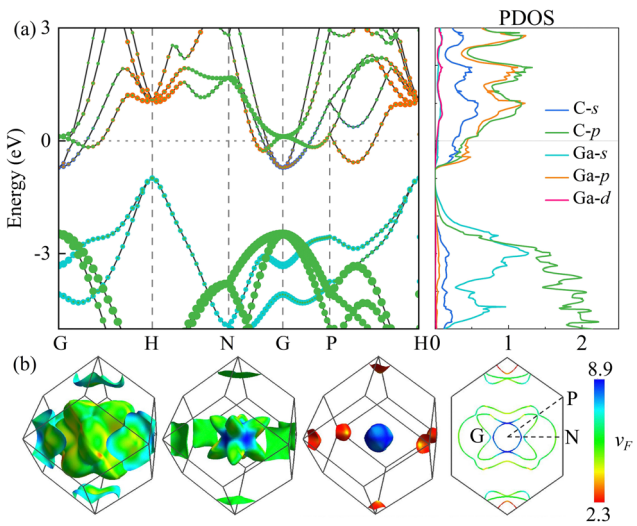

Fig. 2 (a) The calculated electronic band structure and projected DOS (PDOS) for GaC_6. (b) Fermi surface sheets of GaC_6.

The latter exhibits a sizeable gap between bonding and antibonding states of C-s and C-p character. The Ga 4s states are in the occupied/valence region, while the donation of the Ga 4p electron into the C-sublattice leads to partial occupancy of the antibonding C-sp^3 states and therefore metallic character. The electronic DOSs at the Fermi level (N(E_f)) of GaC_6 are primarily contributed by C-s, C-p and Ga-p states. Notably, the aggregate contributions of C-s and C-p states are more than half of the total DOS, which suggests the possibility of strong EPC and the prospect of high temperature superconductivity.[54] We further calculate the projected DOS for Ga d-orbitals. As shown in Fig. S4 (ESI†), the d_{x^2} orbital states of Ga atoms predominate around the Fermi level, exhibiting several peaks. In contrast, the distribution of other d orbitals of Ga atoms is more diffuse, with lower contribution. The Fermi surfaces of GaC_6 are displayed in Fig. 2(b), indicating three electron pockets around the Gamma point. One is very small and the other two are large with multiple bulges. We then calculate the Eliashberg spectral function $\alpha^2F(\omega)$ of GaC_6, which enabled us to obtain the EPC parameters through straightforward frequency domain integration. The results reveal that the EPC parameter λ of GaC_6 at ambient pressure is 1.44, which is larger than the value of 0.7 for MgB_2.[19] The superconducting critical temperatures are estimated by solving the Allen–Dynes modified McMillan (Mc–A–D) equation,[55] the Gor'kov and Kresin (G–K) equation[47,48] and the isotropic Eliashberg (IE) equation[56] (see Table 1). These comprehensive approaches are employed to derive a judicious range of T_c values. Using the Gor'kov and Kresin equation, we estimate the T_c to be 82 K ($\mu^* = 0.1$). Thus, we conduct further analyses of the band structures to find the superconductivity mechanism of GaC_6. Fig. 2(a) illustrates the abundance of electronic states in close proximity to the Fermi level, which elucidate that multiple energy bands cross through it. The energy bands that cross through the Fermi level at the Gamma point are relatively flat, implying that the Fermi velocities approach zero. These flat bands hold the potential to significantly increase the electronic density of states at the Fermi level. Along the N–G–P line, the energy bands crossing the Fermi level in this region are steep, which indicate the large gradients corresponding to high conduction electron velocities.[54] The significant difference in electron velocities at the Fermi level, attributed to the coexistence of energy bands of flat and steep profiles passing through the Fermi level, serves as the catalyst for enhancing the EPC, which is similar to the superconducting mechanism observed in MgB_2.[57,58]

Table 1 Calculated EPC parameters and T_c of GaC_6 and GeC_6 at ambient pressure. The Mc–A–D, G–K and IE correspond to the T_c obtained by the Allen–Dynes modified McMillan equation, the Gor'kov and Kresin equation and the isotropic Eliashberg equation, respectively. The units of ω_{log}, and T_c are Kelvin (K)

	λ_{ac}	λ_{opt}	λ	ω_{log}	$f_1 * f_2$	Mc–A–D	G–K	IE
GaC_6	0.17	1.26	1.44	616.30	1.10	75	82	87
GeC_6	0.32	1.11	1.47	649.38	1.11	60	76	69

To gain a deeper understanding of the superconductivity of GaC_6, we perform calculations of the phonon dispersion curves, phonon density of states (PHDOS), Eliashberg phonon spectral function $\alpha^2F(\omega)$, and integrated EPC $\lambda(\omega)$ (see Fig. 3). The strength of the EPC at given wave vectors and modes λ_{qv} is indicated by the red circles in phonon dispersion curves. Based on the phonon dispersion curves of GaC_6, as shown in Fig. 3(a), a small gap is observed between 4.6 THz and 6.4 THz. The phonon modes below the gap are predominantly contributed by Ga atoms. These are dispersionless "rattling" modes of the Ga atom in the cage, leading – as can be clearly seen from Fig. 3(b) – to a sharp peak in the PHDOS at 4.23 THz. The

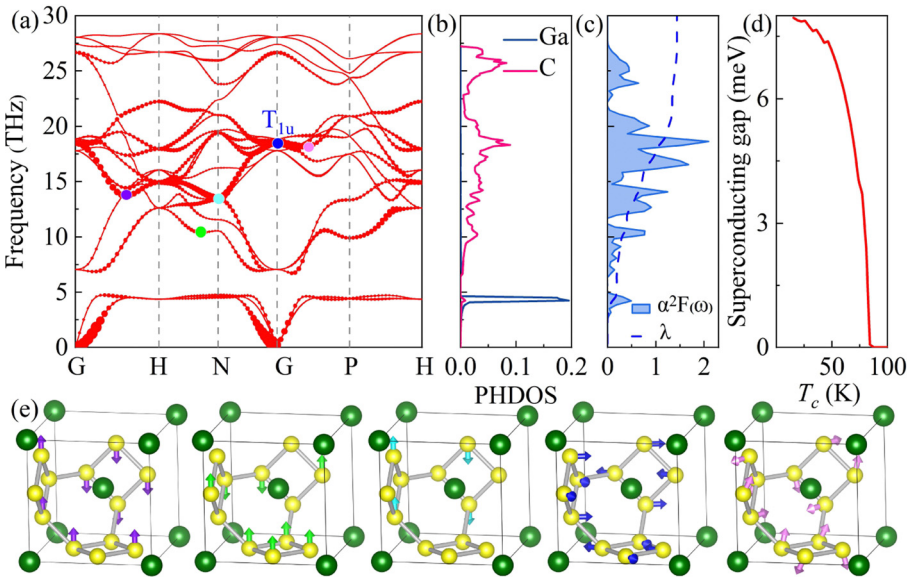

Fig. 3 (a)–(d) Calculated phonon dispersion (the radius of the red circle is proportional to the phonon linewidth), projected phonon density of states (PHDOS), Eliashberg phonon spectral function $\alpha^2F(\omega)$, integrated EPC $\lambda(\omega)$ and calculated superconducting gap for GaC_6 at ambient pressure. (e) Vibration patterns for purple point, green point, azure point, blue point (T_{1u} phonon mode at the Gamma point) and pink point, respectively.

phonon modes above the gap are mostly contributed by C atoms. From Fig. 3(c), it is evident that the medium frequency regions (4.9–22.2 THz) contribute significantly to the EPC, accounting for 79% of the total λ_{qv}. The superconducting gap of GaC_6 is displayed in Fig. 3(d), indicating that the T_c value of GaC_6 is about 87 K under ambient pressure. Interestingly, the T_{1u} phonon mode, characterized by a triple degeneracy and located at the Gamma point, exhibits significant softening and possesses the highest λ_{qv} value and a relatively high frequency (about 18 THz), coupling strongly with electrons. The displacement vector of the T_{1u} phonon mode reveals that the Ga atoms in GaC_6 are relatively inert. Meanwhile, the vibrations of the adjacent C atoms in the C_{24} frameworks strongly stretch the σ bonds between them. Thus, the T_{1u} mode is a three dimensional σ-bond stretching optical mode. In addition to the T_{1u} mode, several other phonon modes with significant softening are also observed, including the phonon mode along the H–N line near 10 THz, the phonon mode along the G–H line near 13 THz, the phonon mode at the N point near 13 THz, and the phonon mode along the G–P line near 17 THz, as shown in Fig. 3(e). These modes correspond to several main peaks of $\alpha^2F(\omega)$, indicating their crucial roles in the EPC interactions. Finally, the phonon modes contributed by C atoms in the high frequency regions contribute about 8% to the EPC.

We now discuss the stability of the $Im\bar{3}m$ – GaC_6 compound. We performed enthalpy calculations for the $Im\bar{3}m$ – GaC_6 across the pressure range of 0 to 80 GPa, including possible decomposition reactions. As shown in Fig. S5 (ESI†), the $Im\bar{3}m$ – GaC_6 was found to have higher enthalpy than the elemental assemblage of diamond and gallium at ambient pressure. The higher energy may stem from strained sp^3 bonds within the sodalite cage. As the pressure increases, the assemblage of C_{60} and gallium would be a potential synthesis route to achieve $Im\bar{3}m$ – GaC_6 at 60 GPa. According to previous studies, SrB_3C_3, possessing a similar strong covalent structure to GaC_6, has been synthesized at near 50 GPa and quenched under ambient conditions in an inert atmosphere.[36,59] Thus, by analogy to other covalent bonded structures that are formed under pressure, these materials may allow metastable persistence under ambient conditions.

GeC_6 compound is another sodalite-like carbon based superconductor with a T_c value of 76 K ($\mu^* = 0.1$) at ambient pressure, which is probably not too surprising given that Ga and Ge are adjacent in the periodic table with similar atomic size and covalent radius.[60] Their electron count differs however, and as a consequence, GeC_6 exhibits the highest charge transfer in this study with approximately 0.8 *e* per Ge atom, but the contributions of Ge-p orbitals at the Fermi level are significant. Additionally, the bands crossing the Fermi level are relatively steep, without the presence of a flat band (see Fig. S6, ESI†). In GeC_6, the conduction band minimum crosses the Fermi level, indicating that GeC_6 is also an electron-doped conductor. As shown in Fig. 4, the Ge atom primarily contributes to the dispersionless rattling modes in the low frequency region, contributing approximately 24% to the EPC. The medium frequency region accounts for 69% of the total λ value contributing to the EPC in GeC_6. The most significant contributor to the EPC in the medium frequency region is the T_{2g} phonon mode located at the Gamma point with a frequency of approximately 19.6 THz. Specifically, the T_{2g} phonon mode is mainly contributed by C atoms. Except for the T_{2g} mode, there are two additional phonon modes that exert notable influence on the λ value, accompanied by observable softening. These modes are identified as follows: the phonon mode along the N–G direction, approximately located at 14.5 THz, and

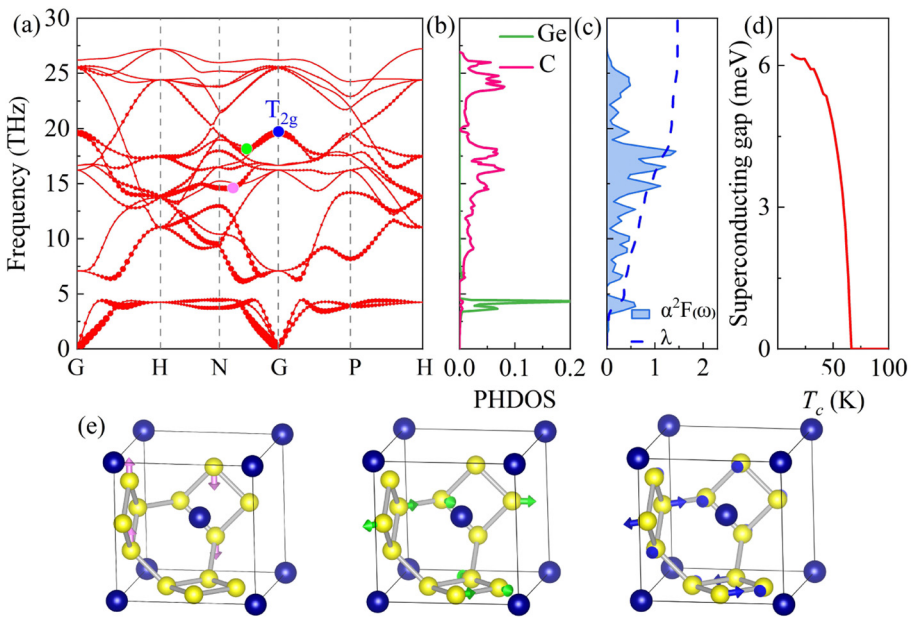

Fig. 4 (a)–(d) Calculated phonon dispersion (the radius of the red circle is proportional to the phonon linewidth), projected phonon density of states (PHDOS), Eliashberg phonon spectral function $\alpha^2F(\omega)$, integrated EPC $\lambda(\omega)$ and calculated superconducting gap for GeC_6 at ambient pressure. (e) Vibration patterns for the pink point, green point and blue point (T_{2g} phonon mode at the Gamma point), respectively.

another phonon mode along the same N–G direction, positioned around 17.6 THz (see Fig. 4). These two modes, in conjunction with the T_{2g} mode, correspond to several prominent peaks of $\alpha^2F(\omega)$, implying their crucial contributions to the EPC and a T_c of 76 K at ambient pressure.

A series of other XC_6 compounds (X = Ni, Cu, Zn, As, Se, Br, Ru, Rh, Pd, Ag, Cd and I) with $Im\bar{3}m$ symmetry are found to be dynamically stable at ambient pressure (see Fig. S1, ESI†). All compounds other than PdC_6, a semiconductor with a band gap of 0.2 eV, are metallic. Tables S2 and S3 (ESI†) summarize the density of states at the Fermi level for each compound, as well as partial charges and predicted T_c. The T_c values for these compounds are lower than those observed in GaC_6 and GeC_6, ranging from 5 to 30 K. The changes in EPC will depend on the guest atom mass and also on the extent of charge transfer and nature of the electronic states at the Fermi level. The free electrons of the C atoms in the C_{24} cages form sp^3 covalent bonds with the other four C atoms, so those electrons are bound within the chemical bonds and cannot participate in conduction. As a result, the pure carbon cage is an insulator, similar to diamond. For more electronegative guest species, the halogens Br and I, the $N(E_f)$ is high: in BrC_6 it is the highest among all XC_6 compounds, reaching 11.84 states/eV/cell. But the Br atom transfers only 0.08 e to the C_{24} cage, which is insufficient to provide enough electrons for the C_{24} cage, resulting in a low T_c of 5 K. For transition metals, $N(E_f)$ can also be high, for example in NiC_6 the $N(E_f)$ is 10.87 states/eV/cell, but the electronic DOSs at the Fermi level predominantly originate from Ni-d orbitals (see Fig. S3, ESI†). The calculated T_c value of the NiC_6 compound is 13 K, implying that partially filled d-shells and therefore an abundance of X-d states at the Fermi level may not be promising for strong EPC and the potential for superconductivity. This is similar to the situation in lanthanide superhydrides.[21]

4 Conclusions

In summary, we employ high-throughput DFT calculations to investigate sodalite-like carbon based superconductors at ambient pressure for a wide range of potential guest atom species. Two sp^3-bonded C_{24} clathrates of GaC_6 and GeC_6 are found to be excellent superconductors with T_c values near to and above the boiling point of liquid nitrogen. The guest Ga and Ge atoms enhance the structural stability of the C_{24} cage while concomitantly acting as the electron donors, which regulates the electronic properties of the C_{24} covalent frameworks. The calculated results elucidate that the abundance of electronic states contributed by C atoms near the Fermi level and the obvious discrepancies of the electron velocities at the Fermi level, corresponding to the ''flat-bands/steep-bands'' scenarios, are the key factors to the high temperature superconductivity of GaC_6 and GeC_6 superconductors. These findings enrich the categories of superconductors at ambient pressure and provide crucial insights for further design and synthesis of novel high temperature superconductors.

Author contributions

C. L., S. Y. J. and X. Y. K. provided the idea and designed research. S. Y. J. and X. L. D. completed the first-principles calculations. All authors took part in the analysis of results and discussions of the research. S. Y. J. wrote the manuscript. X. Y. K., C. L., and A. H. edited the manuscript.

Conflicts of interest

There are no conflicts to declare.

Acknowledgements

This work is supported by the National Natural Science Foundation of China (Grant No. 12174352 and 11874043), the Royal Society International Exchange Scheme (Grant No. IEC\NSFC\201359) and the Fundamental Research Funds for the Central Universities, China University of Geosciences (Wuhan) (Grant No. G1323523065).

References

1 H. Kamerlingh Onnes, *Proc. R. Neth. Acad. Arts Sci.*, 1911, **13**, 1093–1113.
2 G. Aschermann, E. Friederich, E. Justi and J. Kramer, *Phys. Z.*, 1941, **42**, 349–360.
3 J. Eisenstein, *Rev. Mod. Phys.*, 1954, **26**, 277–291.
4 Y.-L. Hai, M.-J. Jiang, H.-L. Tian, G.-H. Zhong, W.-J. Li, C.-L. Yang, X.-J. Chen and H.-Q. Lin, *Adv. Sci.*, 2023, 2303639.
5 J. G. Bednorz and K. A. Muller, *Z. Phys. B: Condens. Matter*, 1986, **64**, 189–193.
6 C. Proust and L. Taillefer, *Annu. Rev. Condens. Matter Phys.*, 2019, **10**, 409–429.
7 T. Gu, W. Cui, J. Hao, J. Shi and Y. Li, *J. Mater. Chem. C*, 2023, **11**, 6386–6392.
8 S. Zhang, R. A. Susilo, S. Wan, W. Deng, B. Chen and C. Gao, *J. Mater. Chem. C*, 2023, **11**, 12254–12260.
9 X. Zhong, Y. Sun, T. Iitaka, M. Xu, H. Liu, R. J. Hemley, C. Chen and Y. Ma, *J. Am. Chem. Soc.*, 2022, **144**, 13394–13400.
10 Y. Xi, X. Jing, Z. Xu, N. Liu, Y. Liu, M.-L. Lin, M. Yang, Y. Sun, J. Zhuang, X. Xu, W. Hao, Y. Li, X. Li, X. Wei, P.-H. Tan, Q. Li, B. Liu, S. X. Dou and Y. Du, *J. Am. Chem. Soc.*, 2022, **144**, 18887–18895.
11 M. Rahm, R. Hoffmann and N. W. Ashcroft, *J. Am. Chem. Soc.*, 2017, **139**, 8740–8751.
12 A. P. Drozdov, P. P. Kong, V. S. Minkov, S. P. Besedin, M. A. Kuzovnikov, S. Mozaffari, L. Balicas, F. F. Balakirev, D. E. Graf, V. B. Prakapenka, E. Greenberg, D. A. Knyazev, M. Tkacz and M. I. Eremets, *Nature*, 2019, **569**, 528–531.
13 J. Nagamatsu, N. Nakagawa, T. Muranaka, Y. Zenitani and J. Akimitsu, *Nature*, 2001, **410**, 63–64.
14 H. J. Choi, D. Roundy, H. Sun, M. L. Cohen and S. G. Louie, *Nature*, 2002, **418**, 758–760.
15 K. Sano, Y. Masuda and H. Ito, *J. Phys. Soc. Jpn.*, 2022, **91**, 083703.

16 Z. Tan, H. Zhang, X. Wu, J. Xing, Q. Zhang and J. Zhu, *Phys. Rev. Lett.*, 2023, **130**, 246802.
17 Y. Sun, J. Lv, Y. Xie, H. Liu and Y. Ma, *Phys. Rev. Lett.*, 2019, **123**, 097001.
18 Z. Zhang, T. Cui, M. J. Hutcheon, A. M. Shipley, H. Song, M. Du, V. Z. Kresin, D. Duan, C. J. Pickard and Y. Yao, *Phys. Rev. Lett.*, 2022, **128**, 047001.
19 J. Kortus, I. I. Mazin, K. D. Belashchenko, V. P. Antropov and L. L. Boyer, *Phys. Rev. Lett.*, 2001, **86**, 4656–4659.
20 S. Di Cataldo, S. Qulaghasi, G. B. Bachelet and L. Boeri, *Phys. Rev. B*, 2022, **105**, 064516.
21 W. Sun, X. Kuang, H. D. J. Keen, C. Lu and A. Hermann, *Phys. Rev. B*, 2020, **102**, 144524.
22 B. Chen, L. J. Conway, W. Sun, X. Kuang, C. Lu and A. Hermann, *Phys. Rev. B*, 2021, **103**, 035131.
23 X. Dou, X. Kuang, W. Sun, G. Jiang, C. Lu and A. Hermann, *Phys. Rev. B*, 2021, **104**, 224510.
24 W. Sun, B. Chen, X. Li, F. Peng, A. Hermann and C. Lu, *Phys. Rev. B*, 2023, **107**, 214511.
25 A. P. Drozdov, M. I. Eremets, I. A. Troyan, V. Ksenofontov and S. I. Shylin, *Nature*, 2015, **525**, 73–76.
26 F. Peng, Y. Sun, C. J. Pickard, R. J. Needs, Q. Wu and Y. Ma, *Phys. Rev. Lett.*, 2017, **119**, 107001.
27 Z. M. Geballe, H. Liu, A. K. Mishra, M. Ahart, M. Somayazulu, Y. Meng, M. Baldini and R. J. Hemley, *Angew. Chem., Int. Ed.*, 2018, **57**, 688–692.
28 M. Somayazulu, M. Ahart, A. K. Mishra, Z. M. Geballe, M. Baldini, Y. Meng, V. V. Struzhkin and R. J. Hemley, *Phys. Rev. Lett.*, 2019, **122**, 027001.
29 Y. Song, J. Bi, Y. Nakamoto, K. Shimizu, H. Liu, B. Zou, G. Liu, H. Wang and Y. Ma, *Phys. Rev. Lett.*, 2023, **130**, 266001.
30 Y. Saito, H. Shinohara, M. Kato, H. Nagashima, M. Ohkohchi and Y. Ando, *Chem. Phys. Lett.*, 1992, **189**, 236–240.
31 O. Gunnarsson, *Rev. Mod. Phys.*, 1997, **69**, 575–606.
32 Y. Iwasa and T. Takenobu, *J. Phys.: Condens. Matter*, 2003, **15**, R495.
33 T. T. M. Palstra, O. Zhou, Y. Iwasa, P. E. Sulewski, R. M. Fleming and B. R. Zegarski, *Solid State Commun.*, 1995, **93**, 327–330.
34 F. Zipoli, M. Bernasconi and G. Benedek, *Phys. Rev. B: Condens. Matter Mater. Phys.*, 2006, **74**, 205408.
35 N. Geng, K. P. Hilleke, L. Zhu, X. Wang, T. A. Strobel and E. Zurek, *J. Am. Chem. Soc.*, 2023, **145**, 1696–1706.
36 L. Zhu, G. M. Borstad, H. Liu, P. A. Gunka, M. Guerette, J.-A. Dolyniuk, Y. Meng, E. Greenberg, V. B. Prakapenka, B. L. Chaloux, A. Epshteyn, R. E. Cohen and T. A. Strobel, *Sci. Adv.*, 2020, **6**, eaay8361.
37 A. Ker, E. Todorov, R. Rousseau, K. Uehara, F.-X. Lannuzel and J. S. Tse, *Chem. – Eur. J.*, 2002, **8**, 2787–2798.
38 N. Rey, A. Munoz, P. Rodriguez-Hernandez and A. S. Miguel, *J. Phys.: Condens. Matter*, 2008, **20**, 215218.
39 S. Lu, H. Liu, I. I. Naumov, S. Meng, Y. Li, J. S. Tse, B. Yang and R. J. Hemley, *Phys. Rev. B*, 2016, **93**, 104509.
40 J. Lv, Y. Wang, L. Zhu and Y. Ma, *J. Chem. Phys.*, 2012, **137**, 084104.
41 Y. Wang, J. Lv, L. Zhu and Y. Ma, *Phys. Rev. B: Condens. Matter Mater. Phys.*, 2010, **82**, 094116.
42 J. Hafner, *Comput. Phys. Commun.*, 2007, **177**, 6–13.
43 J. P. Perdew, K. Burke and M. Ernzerhof, *Phys. Rev. Lett.*, 1996, **77**, 3865–3868.
44 G. Kresse and D. Joubert, *Phys. Rev. B: Condens. Matter Mater. Phys.*, 1999, **59**, 1758–1775.
45 A. Togo and I. Tanaka, *Scr. Mater.*, 2015, **108**, 1–5.
46 P. Giannozzi, S. Baroni, N. Bonini, M. Calandra, R. Car, C. Cavazzoni, D. Ceresoli, G. L. Chiarotti, M. Cococcioni, I. Dabo, A. D. Corso, S. de Gironcoli, S. Fabris, G. Fratesi, R. Gebauer, U. Gerstmann, C. Gougoussis, A. Kokalj, M. Lazzeri, L. Martin-Samos, N. Marzari, F. Mauri, R. Mazzarello, S. Paolini, A. Pasquarello, L. Paulatto, C. Sbraccia, S. Scandolo, G. Sclauzero, A. P. Seitsonen, A. Smogunov, P. Umari and R. M. Wentzcovitch, *J. Phys.: Condens. Matter*, 2009, **21**, 395502.
47 L. P. Gor'kov and V. Z. Kresin, *Sci. Rep.*, 2016, **6**, 25608.
48 L. P. Gor'kov and V. Z. Kresin, *Rev. Mod. Phys.*, 2018, **90**, 011001.
49 A. D. Becke and K. E. Edgecombe, *J. Chem. Phys.*, 1990, **92**, 5397–5403.
50 A. Savin, O. Jepsen, J. Flad, O. K. Andersen, H. Preuss and H. G. von Schnering, *Angew. Chem., Int. Ed. Engl.*, 1992, **31**, 187–188.
51 R. F. W. Bader, *Atoms in Molecules: A Quantum Theory*, Oxford University Press, Oxford, 1994.
52 R. Dronskowski and P. E. Bloechl, *J. Phys. Chem.*, 1993, **97**, 8617–8624.
53 S. Maintz, V. L. Deringer, A. L. Tchougreeff and R. Dronskowski, *J. Comput. Chem.*, 2013, **34**, 2557–2567.
54 A. Simon, *Angew. Chem., Int. Ed. Engl.*, 1997, **36**, 1788–1806.
55 P. B. Allen and R. C. Dynes, *Phys. Rev. B: Solid State*, 1975, **12**, 905–922.
56 G. M. Eliashberg, *J. Exp. Theor.*, 1960, **11**, 696–702.
57 A. Bussmann-Holder, J. Kohler, M. H. Whangbo, A. Bianconi and A. Simon, *Nov. Supercond. Mater.*, 2016, **2**, 37–42.
58 S. Deng, A. Simon and J. Köhler, *Int. J. Mod. Phys. B*, 2005, **19**, 29–36.
59 L. Zhu, H. Liu, M. Somayazulu, Y. Meng, P. A. Guńka, T. B. Shiell, C. Kenney-Benson, S. Chariton, V. B. Prakapenka, H. Yoon, J. A. Horn, J. Paglione, R. Hoffmann, R. E. Cohen and T. A. Strobel, *Phys. Rev. Res.*, 2023, **5**, 013012.
60 B. Cordero, V. Gomez, A. E. Platero-Prats, M. Reves, J. Echeverria, E. Cremades, F. Barragan and S. Alvarez, *Dalton Trans.*, 2008, 2832–2838.

